GEOLOGY | THE GEOLOGICAL SOCIETY OF AMERICA®

https://doi.org/10.1130/G49475.1

Manuscript received 7 July 2021
Revised manuscript received 22 October 2021
Manuscript accepted 24 October 2021

Published online 5 January 2022

Are fluid inclusions in gypsum reliable paleoenvironmental indicators? An assessment of the evidence from the Messinian evaporites

D. Bigi[1]*, S. Lugli[2], V. Manzi[1] and M. Roveri[1]
[1]Department of Chemistry, Life Sciences and Environmental Sustainability, University of Parma, 43124 Parma, Italy
[2]Department of Chemistry and Geological Sciences, University of Modena and Reggio Emilia, 41125 Modena, Italy

ABSTRACT

The paleosalinity of water from which the gypsum precipitated during the Messinian salinity crisis is a controversial issue. Recent microthermometry studies on primary fluid inclusions in gypsum provided very low salinity values not compatible with precipitation from seawater, and suggested strong mixing between seawater and nonmarine waters enriched in calcium sulfate. We applied a new microthermometric protocol on gypsum crystals from nine Mediterranean sections that were experimentally stretched to measure a larger population of fluid inclusions. The results show salinities ranging from 9 to 238 wt‰ NaCl equivalent, largely falling within the evaporation path of normal seawater. The data from previous studies were obtained mostly from those fluid inclusions capable of nucleating a stable bubble after a weak stretching, which probably correspond to those having a lower salinity acquired through post-depositional crack-and-seal processes. Our data suggest instead that the primary gypsum precipitated from a marine brine, later modified by post-trapping processes during tectonics and exhumation.

INTRODUCTION

Fluid inclusions (FIs) in marine minerals such as calcite, gypsum, and halite are a very useful tool for the understanding of the depositional environment because they represent microsamples of ancient seawater from which the minerals precipitated. This information can be obtained by microthermometric analyses unless FIs were modified after trapping. This approach has been applied to the primary bottom-grown selenite gypsum accumulated in the Mediterranean Sea during stages 1 and 3 of the Messinian salinity crisis (MSC; CIESM, 2008; Roveri et al., 2014a; Fig. S1 in the Supplemental Material[1]). However, the salinity of the water body from which the evaporites precipitated is still debated. Several FI studies (Attia et al., 2004; Natalicchio et al., 2014; Evans et al., 2015; Costanzo et al., 2019) led to the idea that the Messinian evaporites precipitated from low-salinity waters, well below the gypsum precipitation field (GPF) for normal marine evaporites. The hypotheses explaining the origin of these low-salinity waters are complex. Natalicchio et al. (2014) suggested that the source of ions came from dissolution of preexisting gypsum by continental fresh water, but no evidence of previous marginal gypsum deposits has ever been found. Grothe et al. (2020) theorized that the Mediterranean-Paratethys water exchanges at the beginning of the MSC caused the formation of a low-salinity surface layer rich in calcium and sulfate, triggering gypsum precipitation at concentrations as low as 40 wt‰ NaCl equivalent (eq.). Also in this case, the source for the solutes remains unexplained.

Contrasting evidence for the continental origin of the evaporites comes from the isotope geochemistry and the biological content, which point to a significant marine signature (Roveri et al., 2014b). From the MSC onset, the Mediterranean began to develop its own hydrology due to the reduced exchanges with the Atlantic Ocean, but during the arid periods at (sub-)precessional scale, the $^{87}Sr/^{86}Sr$ returned to equilibrium with the global ocean (Reghizzi et al., 2018). Only at stage 3 of the MSC is a signal clearly distinct from the global ocean recorded by evaporites, limestone, molluscs, and ostracods (Fig. S2).

The $\delta^{34}S$ and $\delta^{18}O$ from MSC stage 1 gypsum fall very close to those of Miocene seawater, suggesting precipitation from a mostly marine water body (Müller and Mueller, 1991; Lu and Meyers, 2003; Evans et al., 2015; García-Veigas et al., 2018). These two proxies recorded the periodic marine ingressions in the initial (Lugli et al., 2007) and final stages of the crisis (Longinelli, 1979; Manzi et al., 2009), outlining precessional arid-wet cycles.

In this discussion about the salinity of the parent brine from which gypsum precipitated, some other important aspects appear to be commonly overlooked:

(1) Marine faunal assemblages are found in the shale interbedded in the stage 1 gypsum deposits (Neraudeau et al., 2002; Roveri et al., 2020).

(2) Clear evidence of a Paratethyan water influx is found only in the stage 3 deposits with the development of the "Lago-Mare" brackish-water fauna (Roveri et al., 2008, 2014a).

(3) Huge volumes of evaporites from stage 1 and especially stage 2 (halite) suggest that the only viable source of ions could have been the Atlantic Ocean.

(4) The $\delta^{34}S$ of the gypsum of stage 1 commonly points to a marine origin.

Our study explores a new methodology for assessing the reliability of previous FI analyses. We systematically measured FIs never described before within gypsum crystals. Our revised methodological approach demonstrates

*E-mail: diego.bigi@unipr.it

[1]Supplemental Material. Additional information on the samples (Sr data, geographic and geological settings), a detailed description of the methods, and all microthermometric data obtained in this work. Please visit https://doi.org/10.1130/GEOL.S.17139248 to access the supplemental material, and contact editing@geosociety.org with any questions.

CITATION: Bigi, D., et al., 2022, Are fluid inclusions in gypsum reliable paleoenvironmental indicators? An assessment of the evidence from the Messinian evaporites: Geology, v. 50, p. 454–459, https://doi.org/10.1130/G49475.1

the existence of high-salinity FIs that were not previously reported.

GEOLOGICAL SETTINGS AND SAMPLING

We analyzed 12 samples from 9 stratigraphic sections in different geological contexts throughout the entire Mediterranean Basin from the bottom-grown primary gypsum accumulated during MSC stages 1 and 3 (Fig. S3). Ten samples are from the Primary Lower Gypsum (PLG; stage 1; 5.97–5.60 Ma; Lugli et al., 2010; Manzi et al., 2013) of Spain (Sorbas and Almeria-Nijar Basins), northern Italy (Piedmont, Vena del Gesso, and Adriatic Basins), Sicily (Caltanissetta Basin), Egypt (Al-Barqan area), and Cyprus (Pissouri Basin). Two samples are from the Upper Gypsum (UG; stage 3; 5.55–5.33 Ma; Manzi et al., 2009) collected in Sicily (Caltanissetta Basin) and Cyprus (Tokhni Basin).

MATERIALS AND METHODS

Petrography of Fluid Inclusions

We distinguished two primary time-equivalent FI types aligned along different growth bands of the gypsum crystals merging at the oblique boundary between the dark core and the clear portion of the crystal (Figs. 1A, 1B, and 1F):

(1) Type A: Pyramidal-shaped FIs 10–200 μm across, aligned along the crystal growth surface within the reentrant angle of the swallowtail twin (Fig. 1C), which were analyzed in previous studies.

(2) Type B: Mainly tabular, hexagonal FIs 5–30 μm across (Figs. 1D and 1F) and minor pyramidal and triangular inclusion 5–200 μm across, aligned along the vertical-oriented growth bands parallel to the twin plane; these FIs have not been described in the literature to date.

Microthermometric Analysis

A total of 55 millimeter-sized fragments were obtained by cleaving crystals along the 010 cleavage plane with a razor blade. Microthermometry was conducted on a total of 593 FIs to observe the last ice melting temperature, $T_{m(ice)}$, from primary FIs within lateral growth bands and in the reentrant angle of the twin. The analytical method differs significantly from those of previous studies (Attia et al., 2004; Natalicchio et al., 2014; Evans et al., 2015; Costanzo et al., 2019) that allowed the measurement of only a small portion of the FI population. With respect to these previous works, we ran temperature cycles with larger excursions (from −100 °C to +120 °C) at a faster rate (50 °C/min) to enhance the mechanical stretch to the nucleation of a stable bubble. Performing as many as nine cycles, we dramatically increased the number of measurable FIs compared to previous method, using a stress cycle from −90 °C to +30 °C at rate of 30 °C/min (e.g., Attia et al., 1995). This is because the presence of the bubble is the prerequisite for the microthermometric measurements, otherwise the phase changes cannot be observed (Roedder, 1984). More details on our procedure are provided in the Supplemental Material. After the extreme stretching procedure, we performed the measurement run following the same criterion described by Attia et al. (1995).

RESULTS

The salinity values obtained are shown in Figure 2 and in Tables S2 and S3 (in the Supplemental Material). Overall, the salinities vary from 9‰ to 235‰ (wt‰ NaCl eq.) corresponding to $T_{m(ice)}$ from −0.5 °C to −21.7 °C. Nine samples have average salinity values falling within the GPF and ranging from 123‰ to 160‰. Only three samples (RA16-3, SE11-15, and PISS-2) have average salinities (93‰, 94‰, and 85‰, respectively) below the gypsum saturation point. All samples show a wide range of values (Fig. 2; Figs. S5 and S6). Sample EMOG-13 shows the smallest salinity range (108‰–195‰; Figs. 2B and 4), with all FIs except one having marine values and with the highest frequency around 150‰. Except in sample EMOG-13, the values are concentrated in multiple high-frequency points on the normal distribution curve (Fig. 2B; Fig. S6). However, in samples AL16-4, BQ1+BQ3, MT14_4-3-10, SAB6, and TO-1, two main frequency peaks are clearly distinguished, one within the GPF and the other below (Fig. 4; Fig. S6).

DISCUSSION

Our results from FIs, both the new type (type B) and the type usually measured (type A), show a wide salinity range not matched by previous studies that provided only very low salinity values. The main explanation until now for these low values has been that gypsum precipitated from a water body with a strong mixing of seawater and fresh water enriched in Ca^{2+} and SO_4^{2-}. An alternative process could be an unusual precipitation of gypsum triggered by microbiological activity (Natalicchio et al., 2014). An unexplored, more simple explanation is that FIs were modified after trapping. As shown in Figure 2A, the low-salinity FIs are statistically larger, and many of them show clear signs of modification due to post-trapping processes (leakage, necking-down, recrystallization, etc.; Roedder, 1984), whereas high-salinity FIs are statistically smaller. Fluid inclusions with salinity below the gypsum saturation point (110‰) range in size from 12 to ~12,000 μm², whereas those falling in the GPF are much smaller, from 12 to 720 μm²; however, 99.7% of FIs within the GPF are <600 μm² (Fig. 3). The FIs falling within the GPF actually represent the original parent brine, while those with lower salinity have probably been modified by post-depositional processes. This is because gypsum, unlike other evaporitic minerals, presents a perfect cleavage along the 010 plane, which makes its crystals structurally weak by load-unload cycles or tectonic stress. This weakness allows multiple crack-and-seal cycles, which can promote the introduction of low-salinity late fluids. Larger FIs have a higher probability of being intercepted by crack-and-seal processes along 010 planes than the small ones and thus can be more easily involved in mixing by secondary fluids. The result is that we find low salinities especially in large FIs that show clear signs of modification such as partial dissolution and recrystallization (highlighted in red in Fig. 2). The size of 720 μm² (Fig. 3) appears to be the boundary beyond which it is no longer possible to find salinities falling within the expected range of normal seawater precipitation. The size boundary is probably controlled by the spacing of the crack-and-seal discontinuities. One of the major indicators of post-depositional modification is the presence of FIs with a large salinity range (~10‰–150‰) within a single growth band (e.g., Fig. 1D). There would be no reason for FIs along the same growth band to display different salinities unless they were modified in different proportion according to their size by crack-and-seal processes. The crack-and-seal mechanism may not be identified under the microscope because of the strong tendency of gypsum to grow syntaxially without leaving visible traces.

A comparison between previous studies and this work (Fig. 4) shows how the new data are distributed over a wider salinity range reaching higher values. However, the frequency is not entirely random. Especially in the case of the Piedmont Basin (Fig. 4A), two frequency peaks are clearly recognizable. The peak at lower salinities, below the gypsum saturation point, partially overlaps with the previous data set, while that at the highest salinities falls entirely within the GPF and covers salinities never obtained before. The largest FIs belong to the first peak and could represent the preferentially modified ones, whereas the second peak consists only of the smallest FIs, which preserved the parent brine. The methodology used in the previous works allows measurement of only the low-salinity FIs and therefore does not provide representative data. A more representative methodology is only possible by applying a more intense mechanical stress that can allow enlargement of the population of measurable FIs. Finally, the most surprising result is from the Eraclea Minoa (Sicily) Upper Gypsum sample, from which all the values except one fall within the GPF. This is very impressive because the $^{87}Sr/^{86}Sr$ data from MSC stage 3 show the largest proportion of nonmarine waters mixing with seawater. This because $^{87}Sr/^{86}Sr$ is independent of salinity. Our results are in agreement with the scenario of seasonal

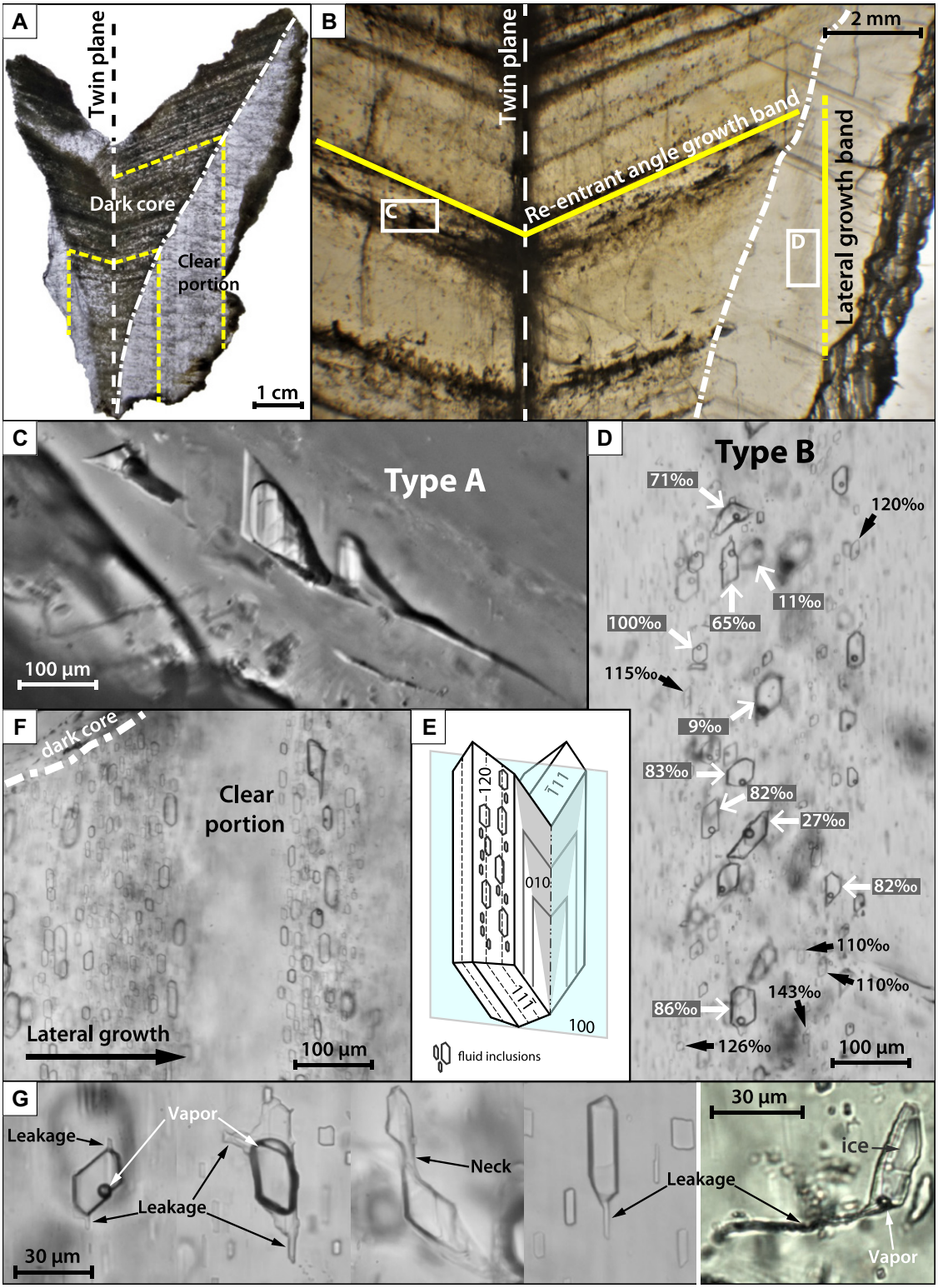

Figure 1. (A) Growth mode of a swallowtail gypsum crystal. Yellow lines represent example isochrons within the growing crystal. (B) Crystal growth produces growth bands both in reentrant angle and in the clear portion at the side of the crystal, generating growth bands parallel to the twin plane 100. (C) Classical pyramidal-shaped fluid inclusion (FI) in reentrant angle (type A). (D) FIs showing very different salinities along same lateral growth band (type B); black arrows point to FIs falling within the expected field from seawater, whereas white arrows indicate FIs at lower salinities. FIs at 71‰, 65‰, 27‰, and 86‰ show clear signs of leakage. (E) Perspective view of swallowtail gypsum crystal; larger FIs intercept more 010 cleavage planes. (F) FI trains marking multiple lateral growth bands. (G) Examples of clearly modified FIs (leakage, necking-down, and presence of vapor bubble before any stress cycles).

input of marine waters into the Mediterranean not only during stage 1 but also during stage 3, as suggested by Manzi et al. (2009) and Vasiliev et al. (2017).

To summarize, our interpretation suggests that Messinian gypsum precipitated from a mostly marine water body and that post-depositional processes (crack and seal) introduced secondary low-salinity fluids that modified the parent brine composition inside the primary FIs. This appears to be the most simple and convincing explanation that fits the evolutionary model of the MSC and does not need to introduce complex additional processes, including microbially mediated reactions. To address the timing of the introduction of new fluids, we need further studies. However, our data indicate that the crystals subjected to intra-Messinian mass-wasting gravitational processes and exhumation (Vena del Gesso Basin: Roveri et al., 2006a; Sorbas and Almeria Basins: Omodeo Salé et al., 2012; Roveri et al., 2019; Sicily: Roveri et al., 2006b, 2008; Manzi et al., 2021; Piedmont Basin: Dela Pierre et al., 2007; Cyprus: Manzi et al., 2016) show the largest FI size and yielded the lowest salinity values. Conversely, the strata still buried (Sabbioncello, Italy; Manzi et al., 2020) or

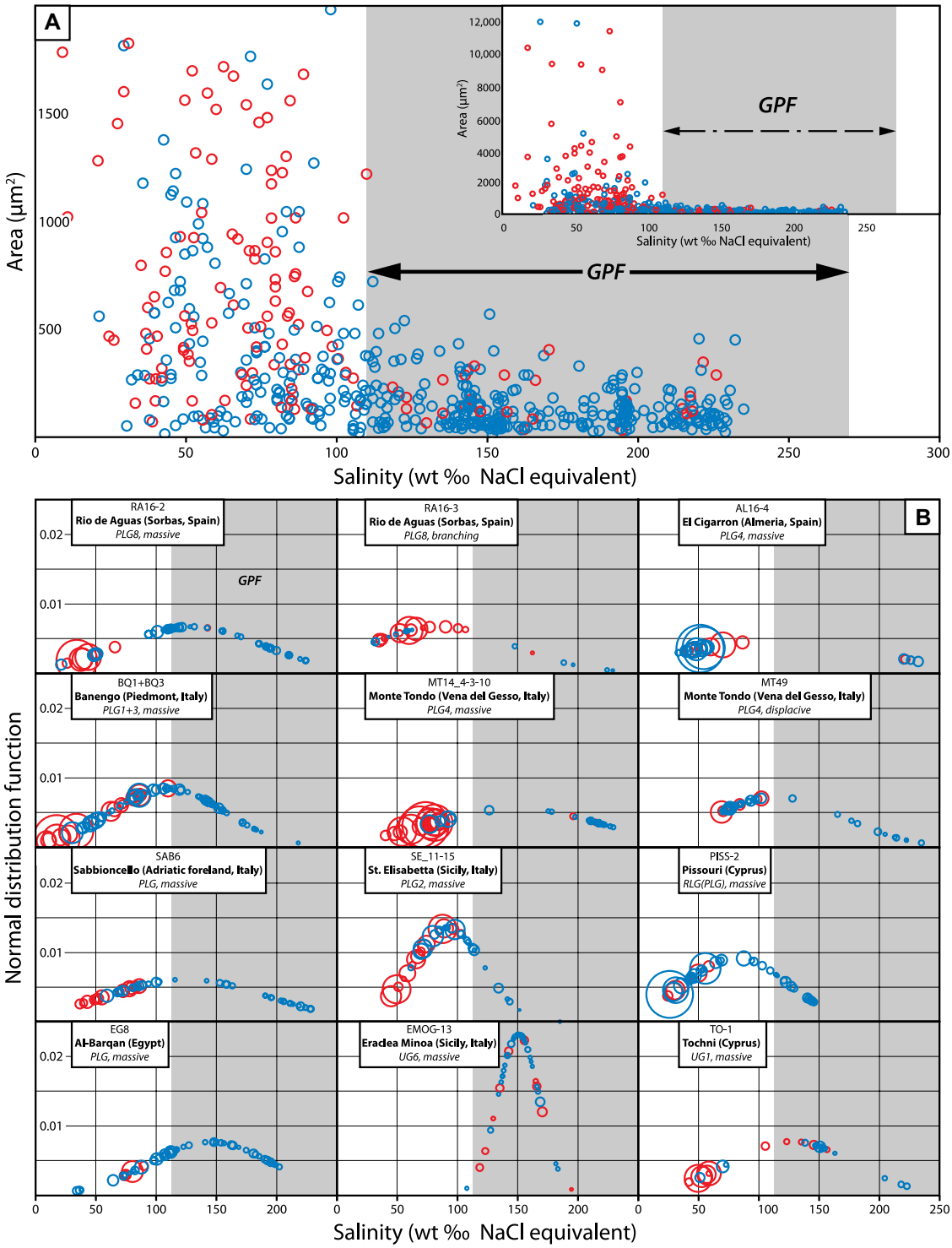

Figure 2. (A) Salinity versus size of all 538 measured fluid inclusions (FIs) (both type A and B). The gypsum saturation threshold (110‰) separates two distinct groups: FIs that fall in the gypsum precipitation field (GPF) of seawater show a small size range (12 to ~700 µm²), whereas those that fall below the 110‰ value show a wider range (12 to ~12,000 µm²). FIs with clear signs of modification (red circles) usually fall below the gypsum saturation field. (B) Plot of function of the normal distribution of salinity for each sample. Circle width is proportional to FI size. Blue circles identify apparently unmodified FI, whereas red circles indicate FI showing clear signs of post-trapping modification (necking down, etc.). PLG—Primary Lower Gypsum; RLG—Resedimented Lower Gypsum; UG—Upper Gypsum.

exhumed during the Quaternary (Eraclea Minoa, Sicily) (Manzi et al., 2009) show the smallest pristine inclusions and the largest proportion of salinity values falling within the GPF. We cannot exclude multiple crack-and-seal phases.

CONCLUSIONS

Each analyzed sample shows a wide salinity range, from low to very high values. The high values fall within the expected range of the evaporation curve from seawater and have not been measured before. The large differences in salinity for FIs lying along the same growth band could only be interpreted via variable post-depositional modification of the trapped primary fluid. This study reveals that gypsum is a mineral unable to best preserve salinity information throughout geological time due to its remarkable crystallographic weakness.

The concept that Messinian gypsum precipitated from a low-salinity water body is probably the result of a strong bias in FI selection and measurement. The data obtained previously do not cover the entire range of FIs originally trapped within the crystals, but only those capable of nucleating a stable bubble after a weak stretching, which are only those having extremely low salinity. However, the low salinity was acquired via post-depositional crack-and-seal processes. The true witness of the depositional environment, i.e., normal precipitation from seawater, are the small FIs, which can be measured only after extreme stretching.

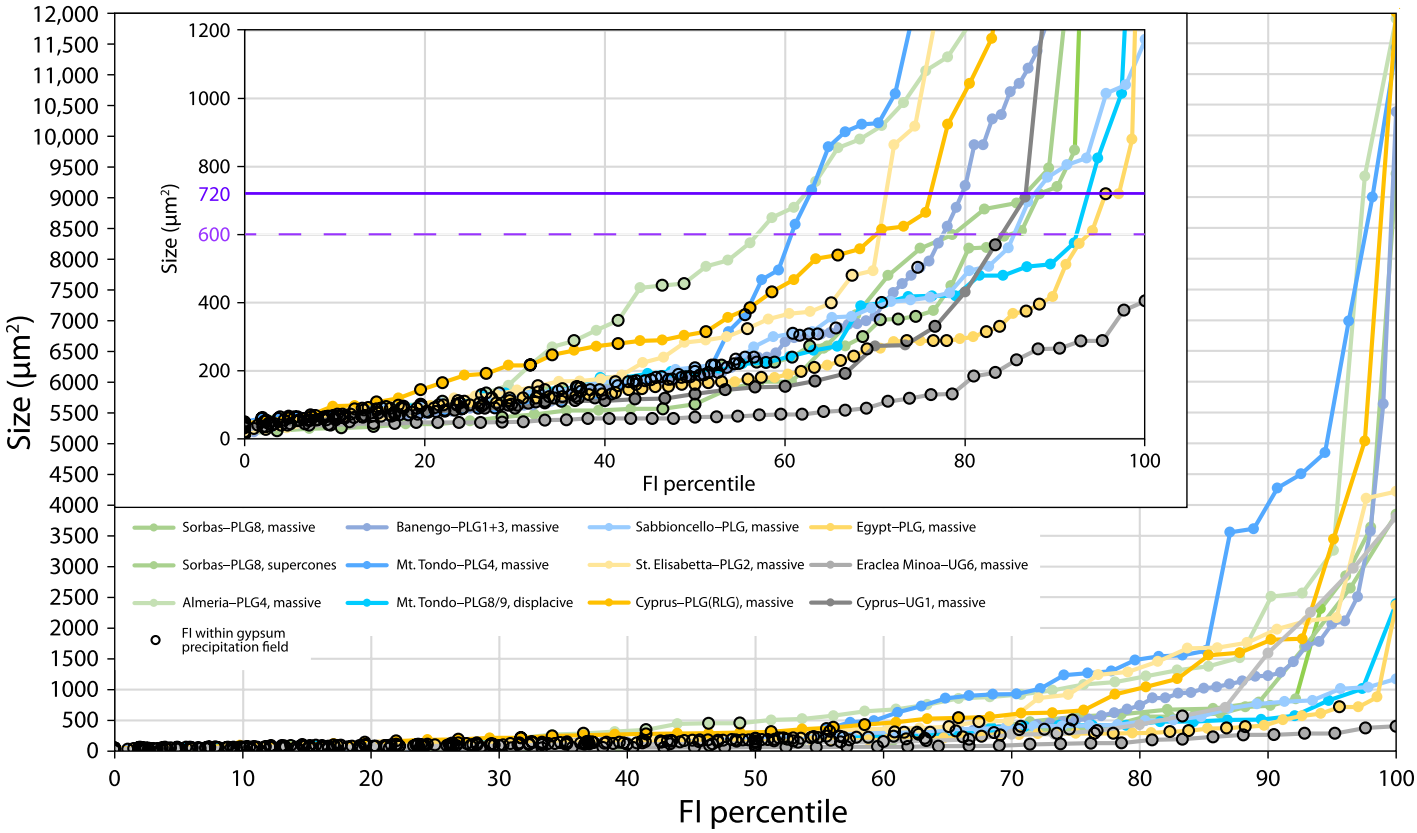

Figure 3. Statistical distribution of fluid inclusion (FI) sizes for each sample. Inset shows an enlargement of the overall graph (in the background) to better show the distribution of the smaller FIs. PLG—Primary Lower Gypsum; RLG—Resedimented Lower Gypsum; UG—Upper Gypsum. Black circles indicate FIs falling within the gypsum precipitation field of normal seawater; most of them (99.7%) are smaller than 600 µm², and largest one reaches 720 µm².

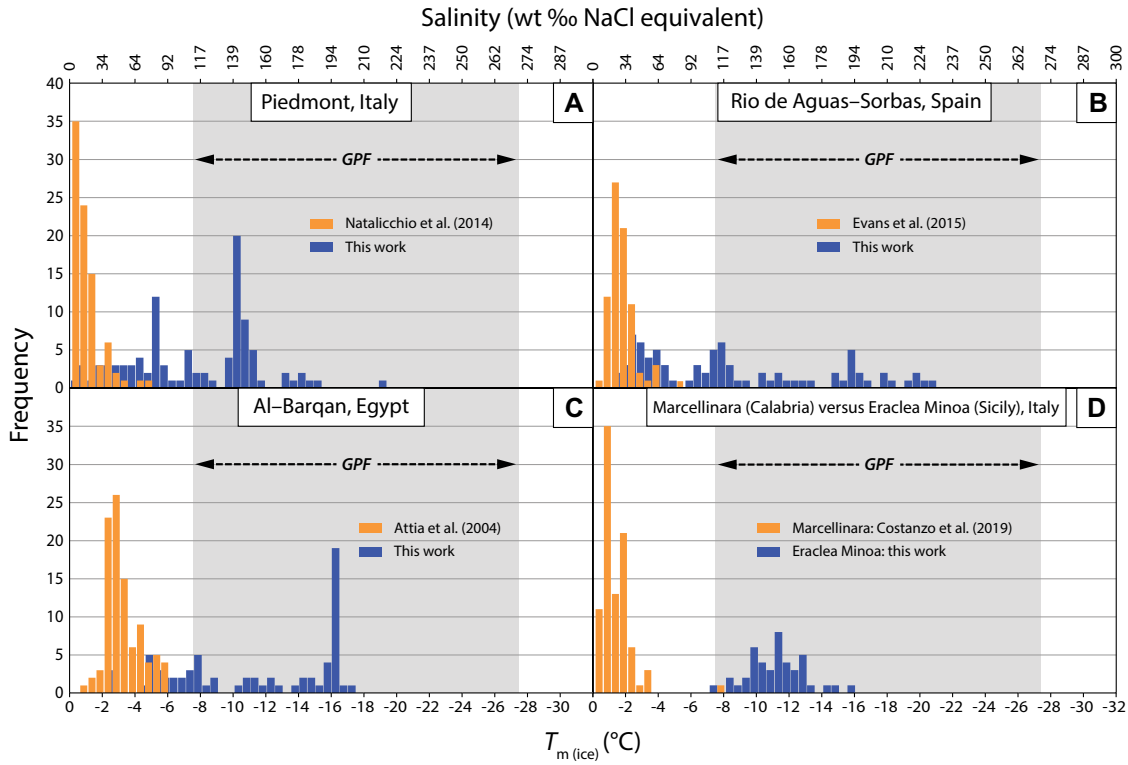

Figure 4. Frequency of last ice melting temperature, $T_{m(ice)}$, classed by 0.5 °C temperature intervals. (A–C) Comparison between previously published (orange) and new data sets (blue) obtained from the same gypsum beds. Our data show higher salinity values and multiple frequency peaks, particularly for the Piedmont Basin. (D) Comparison between Upper Gypsum samples from Marcellinara (Calabria, southern Italy) and Eraclea Minoa (Sicily); note the almost total lack of overlap between the two data sets. GPF—gypsum precipitation field.

If this hypothesis is correct, then another possible implication can be inferred. The definition of the depositional environment of gypsum based on the geochemistry ($\delta^{18}O$ and δD) of the crystallization water could also be affected. This is because the crack-and-seal mechanism may introduce new variable aliquots of water due to the syntaxial growth of gypsum during burial and exhumation.

ACKNOWLEDGMENTS

We thank E. Salvioli Mariani (University of Parma, Italy) for technical support during microthermometric analysis on fluid inclusions, and Ahmed Sadek Mansour (Alexandria University, Egypt) who gave us the sample from Egypt. D.A. Vanko, two anonymous reviewers, and editor G.R. Dickens are acknowledged for helpful suggestions and comments on an early version of the manuscript. This work has benefited from the equipment and framework of the COMP-HUB Initiative, funded by the Departments of Excellence program of the Italian Ministry for Education, University and Research (MIUR, 2018–2022).

REFERENCES CITED

Attia, O.E., Lowenstein, T.K., and Wali, A.M.A., 1995, Middle Miocene gypsum, Gulf of Suez: Marine or nonmarine?: Journal of Sedimentary Research, v. 65A, p. 614–626, https://doi.org/10.1306/D4268176-2B26-11D7-8648000102C1865D.

Attia, O.E., El Khoriby, E.M., and Aref, M.A., 2004, Sedimentology and fluid inclusions criteria of the Upper Miocene (Messinian?) gypsum deposits in the Mediterranean coast of Egypt: Sedimentology of Egypt, v. 12, p. 23–39.

CIESM (Mediterranean Science Commission), 2008, The Messinian Salinity Crisis from mega-deposits to microbiology—A consensus report (Briand, F., ed.): CIESM Workshop Monograph 33, 168 p.

Costanzo, A., Cipriani, M., Feely, M., Cianfione, G., and Dominici, R., 2019, Messinian twinned selenite from the Catanzaro Trough, Calabria, Southern Italy: Field, petrographic and fluid inclusion perspectives: Carbonates and Evaporites, v. 34, p. 743–756, https://doi.org/10.1007/s13146-019-00516-0.

Dela Pierre, F., Festa, A., and Irace, A., 2007, Interaction of tectonic, sedimentary, and diapiric processes in the origin of chaotic sediments: An example from the Messinian of Torino Hill (Tertiary Piedmont Basin, northwestern Italy): Geological Society of America Bulletin, v. 119, p. 1107–1119, https://doi.org/10.1130/B26072.1.

Evans, N.P., Turchyn, A.V., Gázquez, F., Bontognali, T.R.R., Chapman, H.J., and Hodell, D.A., 2015, Coupled measurements of $\delta^{18}O$ and δD of hydration water and salinity of fluid inclusions in gypsum from the Messinian Yesares Member, Sorbas Basin (SE Spain): Earth and Planetary Science Letters, v. 430, p. 499–510, https://doi.org/10.1016/j.epsl.2015.07.071.

García-Veigas, J., Cendón, D.I., Gibert, L., Lowenstein, T.K., and Artiaga, D., 2018, Geochemical indicators in Western Mediterranean Messinian evaporites: Implications for the salinity crisis: Marine Geology, v. 403, p. 197–214, https://doi.org/10.1016/j.margeo.2018.06.005.

Grothe, A., et al., 2020, Paratethys pacing of the Messinian Salinity Crisis: Low salinity waters contributing to gypsum precipitation?: Earth and Planetary Science Letters, v. 532, 116029, https://doi.org/10.1016/j.epsl.2019.116029.

Longinelli, A., 1979, Isotope geochemistry of some Messinian evaporates: Paleoenvironmental implications: Palaeogeography, Palaeoclimatology, Palaeoecology, v. 29, p. 95–123, https://doi.org/10.1016/0031-0182(79)90076-2.

Lu, F.H., and Meyers, W.J., 2003, Sr, S, and O_{SO4} isotopes and the depositional environments of the upper Miocene evaporites, Spain: Journal of Sedimentary Research, v. 73, p. 444–450, https://doi.org/10.1306/093002730444.

Lugli, S., Bassetti, M.A., Manzi, V., Barbieri, M., Longinelli, A., and Roveri, M., 2007, The Messinian 'Vena del Gesso' evaporites revisited: Characterization of isotopic composition and organic matter, *in* Schreiber, B.C., et al., eds., Evaporites Through Space and Time: Geological Society [London] Special Publication 285, p. 179–190, https://doi.org/10.1144/SP285.11.

Lugli, S., Manzi, V., Roveri, M., and Schreiber, B.C., 2010, The Primary Lower Gypsum in the Mediterranean: A new facies interpretation for the first stage of the Messinian salinity crisis: Palaeogeography, Palaeoclimatology, Palaeoecology, v. 297, p. 83–99, https://doi.org/10.1016/j.palaeo.2010.07.017.

Manzi, V., Lugli, S., Roveri, M., and Schreiber, B.C., 2009, A new facies model for the Upper Gypsum (Sicily, Italy): Chronological and paleoenvironmental constraints for the Messinian salinity crisis in the Mediterranean: Sedimentology, v. 56, p. 1937–1960, https://doi.org/10.1111/j.1365-3091.2009.01063.x.

Manzi, V., Gennari, R., Hilgen, F., Krijgsman, W., Lugli, S., Roveri, M., and Sierro, F.J., 2013, Age refinement of the Messinian salinity crisis onset in the Mediterranean: Terra Nova, v. 25, p. 315–322, https://doi.org/10.1111/ter.12038.

Manzi, V., Lugli, S., Roveri, M., Dela Pierre, F., Gennari, R., Lozar, F., Natalicchio, M., Schreiber, B.C., Taviani, M., and Turco, E., 2016, The Messinian salinity crisis in Cyprus: A further step towards a new stratigraphic framework for Eastern Mediterranean: Basin Research, v. 28, p. 207–236, https://doi.org/10.1111/bre.12107.

Manzi, V., Argnani, A., Corcagnani, A., Lugli, S., and Roveri, M., 2020, The Messinian salinity crisis in the Adriatic foredeep: Evolution of the largest evaporitic marginal basin in the Mediterranean: Marine and Petroleum Geology, v. 115, 104288, https://doi.org/10.1016/j.marpetgeo.2020.104288.

Manzi, V., Roveri, M., Argnani, A., Cowan, D., and Lugli, S., 2021, Large-scale mass-transport deposits recording the collapse of an evaporitic platform during the Messinian salinity crisis (Caltanissetta basin, Sicily): Sedimentary Geology, v. 424, 106003, https://doi.org/10.1016/j.sedgeo.2021.106003.

Müller, D.W., and Mueller, P.A., 1991, Origin and age of the Mediterranean Messinian evaporites: Implications from Sr isotopes: Earth and Planetary Science Letters, v. 107, p. 1–12, https://doi.org/10.1016/0012-821X(91)90039-K.

Natalicchio, M., Dela Pierre, F., Lugli, S., Lowenstein, T.K., Feiner, S.J., Ferrando, S., Manzi, V., Roveri, M., and Clari, P., 2014, Did Late Miocene (Messinian) gypsum precipitate from evaporated marine brines? Insights from the Piedmont Basin (Italy): Geology, v. 42, p. 179–182, https://doi.org/10.1130/G34986.1.

Neraudeau, D., Courville, P., Goubert, E., and Rouchy, J.-M., 2002, Corrélation des niveaux fossilifères marins interstratifies dans les gypses messiniens, entre la carrière de Los Yesos et la carrière de Molinos de Aguas (bassin de Sorbas, SE Espagne): Geodiversitas v. 24, p. 659–667.

Omodeo Salé, S., Gennari, R., Lugli, S., Manzi, V., and Roveri, M., 2012, Tectonic and climatic control on the Late Messinian sedimentary evolution of the Nijar Basin (Betic Cordillera, Southern Spain): Basin Research, v. 24, p. 314–337, https://doi.org/10.1111/j.1365-2117.2011.00527.x.

Reghizzi, M., Lugli, S., Manzi, V., Rossi, F.P., and Roveri, M., 2018, Orbitally forced hydrological balance during the Messinian Salinity Crisis: Insights from strontium isotopes ($^{87}Sr/^{86}Sr$) in the Vena del Gesso Basin (Northern Apennines, Italy): Paleoceanography and Paleoclimatology, v. 33, p. 716–731, https://doi.org/10.1029/2018PA003395.

Roedder, E., 1984, Interpretation and utilization of inclusion measurements—Metastability, *in* Roedder, E., ed., 1984, Fluid Inclusions: Mineralogical Society of America Reviews in Mineralogy 12, p. 291–323, https://doi.org/10.1515/9781501508271-013.

Roveri, M., Manzi, V., Ricci Lucchi, F., and Rogledi, S., 2003, Sedimentary and tectonic evolution of the Vena del Gesso Basin (Northern Apennines, Italy): Implications for the onset of the Messinian salinity crisis: Geological Society of America Bulletin, v. 115, p. 387–405, https://doi.org/10.1130/0016-7606(2003)115<0387:SATEOT>2.0.CO;2.

Roveri, M., Lugli, S., Manzi, V., Gennari, R., Iaccarino, S.M., Grossi, F., and Taviani, M., 2006a, The record of Messinian events in the Northern Apennines foredeep basins: Acta Naturalia de L'Ateneo Parmense, v. 42, p. 47–123.

Roveri, M., Manzi, V., Lugli, S., Schreiber, B.C., Caruso, A., Rouchy, J.-M., Iaccarino, S.M., Gennari, R., Vitale, F.P., and Ricci Lucchi, F., 2006b, Clastic vs. primary precipitated evaporites in the Messinian Sicilian basins: Acta Naturalia de L'Ateneo Parmense, v. 42, p. 125–199.

Roveri, M., et al., 2008, A high-resolution stratigraphic framework for the latest Messinian events in the Mediterranean area: Stratigraphy, v. 5, p. 323–342.

Roveri, M., et al., 2014a, The Messinian Salinity Crisis: Past and future of a great challenge for marine sciences: Marine Geology, v. 352, p. 25–58, https://doi.org/10.1016/j.margeo.2014.02.002.

Roveri, M., Lugli, S., Manzi, V., Gennari, R., and Schreiber, B.C., 2014b, High-resolution strontium isotope stratigraphy of the Messinian deep Mediterranean basins: Implications for marginal to central basins correlation: Marine Geology, v. 349, p. 113–125, https://doi.org/10.1016/j.margeo.2014.01.002.

Roveri, M., Gennari, R., Persico, D., Rossi, F.P., Lugli, S., Manzi, V., Reghizzi, M., and Taviani, M., 2019, A new chronostratigraphic and palaeoenvironmental framework for the end of the Messinian salinity crisis in the Sorbas Basin (Betic Cordillera, southern Spain): Geological Journal, v. 54, p. 1617–1637, https://doi.org/10.1002/gj.3256.

Roveri, M., Lugli, S., Manzi, V., Reghizzi, M., and Rossi, F.P., 2020, Stratigraphic relationships between shallow-water carbonates and primary gypsum: Insights from the Messinian succession of the Sorbas Basin (Betic Cordillera, Southern Spain): Sedimentary Geology, v. 404, 105678, https://doi.org/10.1016/j.sedgeo.2020.105678.

Vasiliev, I., Mezger, E., Lugli, S., Reichart, G.J., Manzi, V., and Roveri, M., 2017, How dry was the Mediterranean during the Messinian salinity crisis?: Palaeogeography, Palaeoclimatology, Palaeoecology, v. 471, https://doi.org/10.1016/j.palaeo.2017.01.032.

Printed in USA